Computer modeling of acoustic beam formation in *Delphinus delphis*

James L. Aroyan
Institute for Nonlinear Science, 307 Natural Sciences II, University of California, Santa Cruz, California 95064

Ted W. Cranford
Long Marine Laboratory, University of California, Santa Cruz, California 95064

Joel Kent
Elographics, 41752 Christy Street, Fremont, California 94538

Kenneth S. Norris
Long Marine Laboratory, University of California, Santa Cruz, California 95064

(Received 17 June 1991; accepted for publication 25 June 1992)

It has been established that some dolphins possess well-developed acoustic orientation (echolocation) and information gathering abilities, though substantially less is known about the system of sound generation and beam formation. Dolphins use a narrowly focused sound beam that emanates from the forehead and rostrum during echolocation. The primary objectives of this study were to simulate the effects of anatomical structure on beam formation, and to test the viability of various hypothetical sound source locations. Outlines from parasagittal x-ray CT scans were used to construct a 2-D model of the head of the common dolphin, *Delphinus delphis*. Finite difference techniques were used to simulate sound propagation through tissues modeled as inhomogeneous fluids. Preliminary simulations confirm that beam formation results primarily from reflection off of the skull and the skull-supported air sac surfaces. For the frequencies tested, beam angles best approximate those measured by experimental methods for a source located in a region of the model referred to as the monkey lip/dorsal bursae (MLDB) complex. The results suggest that: (1) the skull and air sacs play the central role in beam formation; (2) the geometry of reflective tissue is more important than the exact acoustical properties assigned; (3) a melon velocity profile of the magnitude tested is capable of mild focusing effects; and (4) experimentally observed beam patterns are best approximated at all frequencies simulated when the sound source is placed in the vicinity of the MLDB complex.

PACS numbers: 43.80.Ka, 43.80.Lb, 43.80.Nd

INTRODUCTION

It has been established that some dolphins possess a highly sophisticated and adaptable sonar system, though substantially less is known about the system of sound generation and beam formation. Measurements[1] of the acoustic field of echolocating dolphins have demonstrated that dolphins emit a rapid series of clicks in a narrowly focused beam which emanates from the forehead and rostrum during echolocation. For an Atlantic bottlenose dolphin, Au *et al.* (1986) found the major axis of the echolocation beam pattern in the vertical direction to be elevated at 5 deg above the reference axis of the upper jaw, and reported a -3-dB vertical beamwidth of approximately 5–7 deg for the composite broadband pattern. Though details of sound source location and operation remain conjectural, several experimental methodologies have implicated the region of the upper (supranarial) nasal passages as the site of echolocation click production (see Sec. III B). In addition, investigators have studied the role of the skull and/or soft tissues in beam formation using acoustic sources with real tissues (Evans *et al.*, 1964; Norris and Harvey, 1974; Romanenko, 1974), light sources and ray-tracing techniques (Evans *et al.*, 1964; Dubrovkiy and Zaslavskiy, 1975; Litchfield *et al.*, 1979), and topographic chemical and/or acoustic lipid analyses (Norris and Harvey, 1974; Litchfield *et al.*, 1979; Varanasi *et al.*, 1981). Experimental procedures for determining the interactions of tissues and acoustic sources offer certain advantages yet are often difficult to implement, while the validity of light source and ray-tracing techniques are limited by the range of wavelengths involved.

This report presents results from the initial stages of an alternative and complementary approach to the experimental investigation of echolocation hypotheses, which allows the effects of modeled tissues to be studied in arbitrary combination. The objectives of this study were to numerically simulate the effects of delphinid tissues on beam formation, and to test the viability of various hypothetical sound source locations. Two-dimensional simulations of sound propagation through modeled forehead tissues of the common dolphin, *Delphinus delphis*, were used to investigate the interaction of the skull with various source locations, and to investigate the roles of the skull, air passages, and the fatty melon on the formation of acoustic beams.

 0001-4966/92/112539-07$00.80

I. COMPUTATIONAL METHODS

Propagation of sound through biological tissues may be approximated by numerical integration of the acoustic wave equation.[2] Though biological tissues are composed of intermixed fluids and elastic solids, the shear modulus of most tissues (except bone) is small. The acoustic impedance mismatch between bone and soft tissue[3] and the fact that air sacs cover much of the skull surface in the region of the dolphin's nasal passages suggest that little shear wave energy can be generated by a soft tissue sound source. In these simulations, tissues (including bone) were modeled as inhomogeneous fluids and shear wave modes were ignored.

In fluids of inhomogeneous velocity and density, the linearized wave equation for acoustic pressure p is[4]

$$\frac{1}{c^2(\mathbf{x})\rho_0(\mathbf{x})}\frac{\partial^2 p}{\partial t^2} = \nabla\cdot\left(\frac{\nabla p}{\rho_0(\mathbf{x})}\right), \tag{1}$$

where velocity c and background density ρ_0 are both functions of position $\mathbf{x}$. By mapping the positions of the tissues onto a grid and assigning values of tissue velocity and density, finite differencing schemes can be used to propagate the solution of Eq. (1) forward in time, allowing investigation of the beam pattern formed by various models of tissue and source configuration. The discrete version of Eq. (1) applied over tissue regions of the grid and other computational details are presented in the Appendix.

For this project, a parasagittal x-ray computed tomogram (CT) of the head of the dolphin, *Delphinus delphis*, was enlarged and used to trace tissue outlines onto a digitizing tablet. The resulting coordinate sets were scaled and mapped onto a square grid (increment size $h = 1.5$ mm), with tissue velocity and density values estimated from the literature. Programs were run on a supercomputer with run times of between 4 and 8 min per simulation. Grid dispersion dictates a wavelength minimum of about five grid increments (Alford *et al.*, 1974), setting an upper frequency bound of approximately 200 kHz in these simulations.

Two types of simulation results are presented below. Figures 1 and 7 are (time-averaged) energy flux vector diagrams illustrating grid setup. The length and direction of the vectors provide a quick visualization of the intensity and direction of energy flow in a simulation. Another type of result is generated from amplitude records taken at the ring of points surrounding the tissue regions in Figs. 1 and 7. Plots of the mean-square amplitude at these points versus angle are collected in Figs. 3, 4, 6, and 8 to give (linear) polar plots of acoustic energy flow in the simulations,[5] which may be compared to experimentally measured beam patterns.

II. MODEL OF THE DOLPHIN

For our model of the dolphin, *Delphinus delphis*, tissue geometry information was derived from a CT scan as described above, and values of velocity and density were estimated from the literature.[6] Variations in velocity and density over soft tissue regions (except the melon) were neglected,[7] though these variations may be of importance to the dolphin.[8]

The sound-speed measurements of Norris and Harvey (1974) on the melon of a Pacific bottlenose dolphin were fed

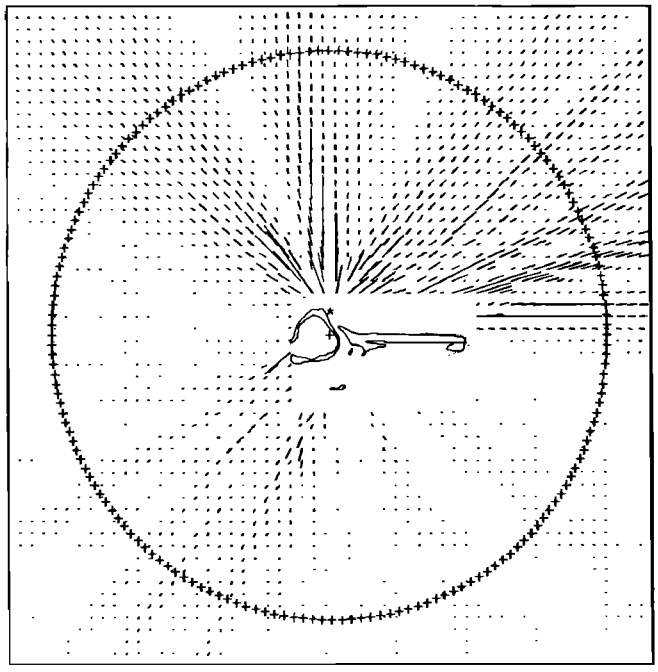

FIG. 1. Skull-only simulation. Average energy flux vector diagram illustrating grid setup and acoustic energy flow in a simulation with a point source of frequency 100 kHz located in the MLDB complex. Outlines of simulated tissues are traced in the center of the display (skin outlines are included for visual reference only). Source position is marked with a five-pointed star.

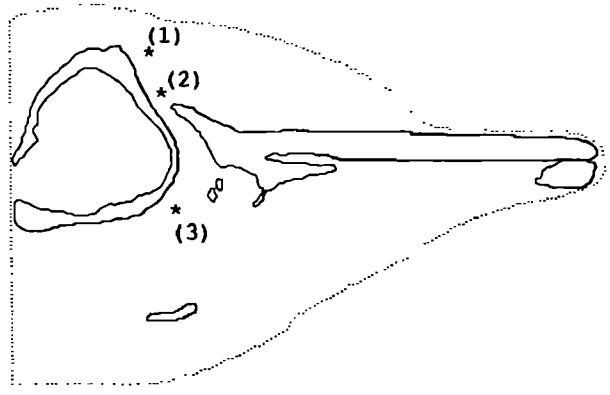

FIG. 2. Source positions. Source positions used in the simulations are marked: (1) for the MLDB complex; (2) for the nasal plug area; and (3) for the region of the larynx. The modeled skull (solid) and skin (dotted) outlines are pictured.

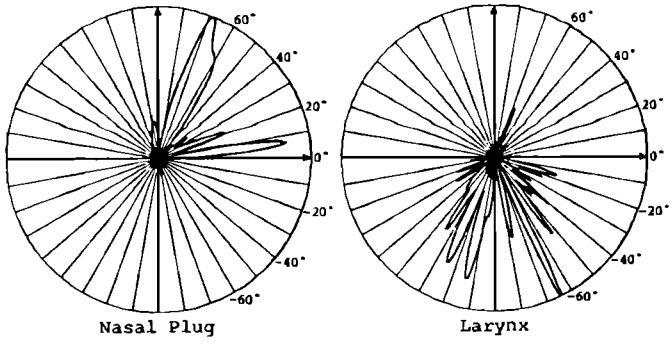

FIG. 3. Moved source simulations. Linear polar plots of acoustic intensity (mean-square amplitude) for 100-kHz point sources placed at the position of the nasal plugs (left) and in the region of the larynx (right) in the skull-only model.

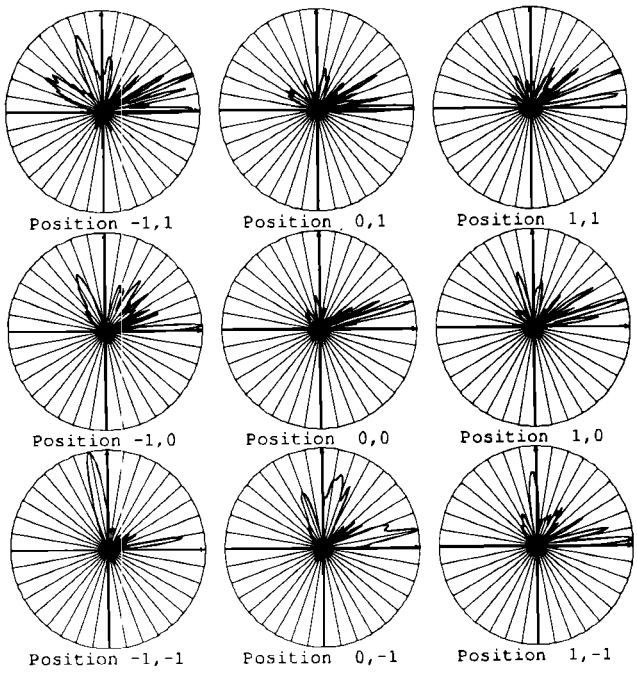

FIG. 4. MLDB moved source simulations. Linear polar plots of acoustic intensity (mean square amplitude) for small displacements of a 100-kHz point source about the MLDB complex in the skull-only model. Positions correspond to increments of 0.75 cm on a grid placed over the MLDB region; e.g., source position 1,1 is shifted both forward and upward by 0.75 cm from the center of the MLDB.

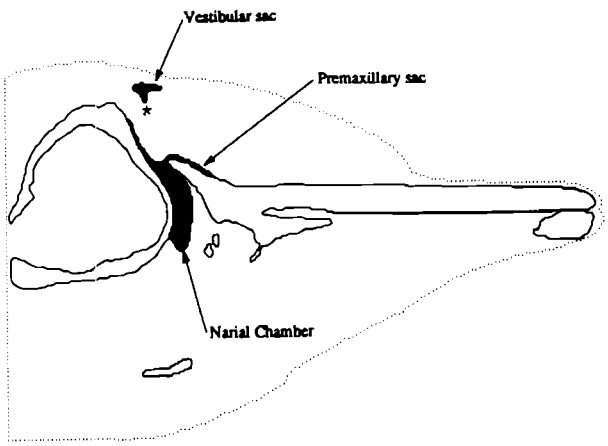

FIG. 5. Diagram of the *Delphinus* air sac model used in the simulations; air sacs are darkened. Also pictured are the modeled skull (solid) and skin (dotted) outlines. The MLDB source position is marked with a five-pointed star.

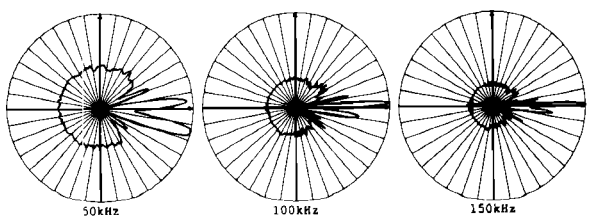

FIG. 6. Melon-only simulations. Linear polar plots of acoustic intensity from simulations of the effect of the melon velocity profile alone (no other tissues) on MLDB sources of 50, 100, and 150 kHz.

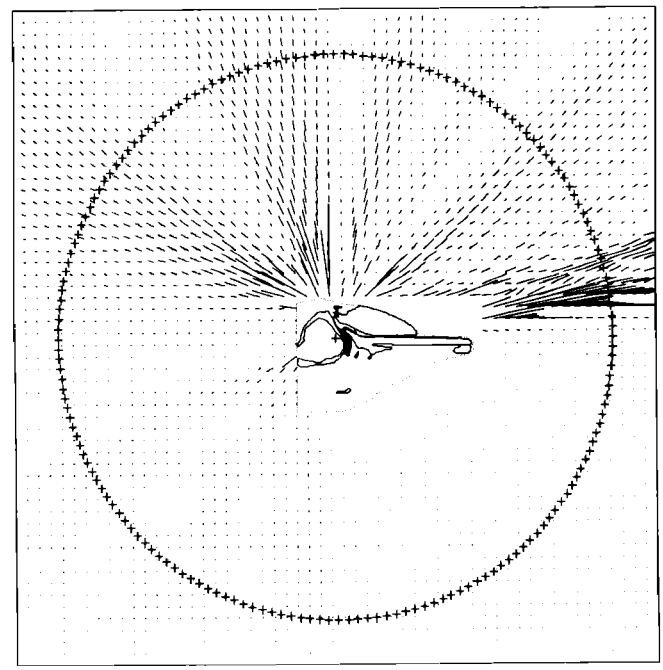

FIG. 7. Skull, air sacs, and melon simulation. Average energy flux vector diagram illustrating grid setup and acoustic energy flow in a 100-kHz MLDB source simulation. Skull and melon region are outlined (solid), and air sacs are darkened. Source position is marked with a five-pointed star.

into a contouring program to generate a melon velocity profile.[9] Though sparse and unfortunately not from *Delphinus*, this profile can be used to qualitatively investigate the effectiveness of the melon tissues in focusing sound.

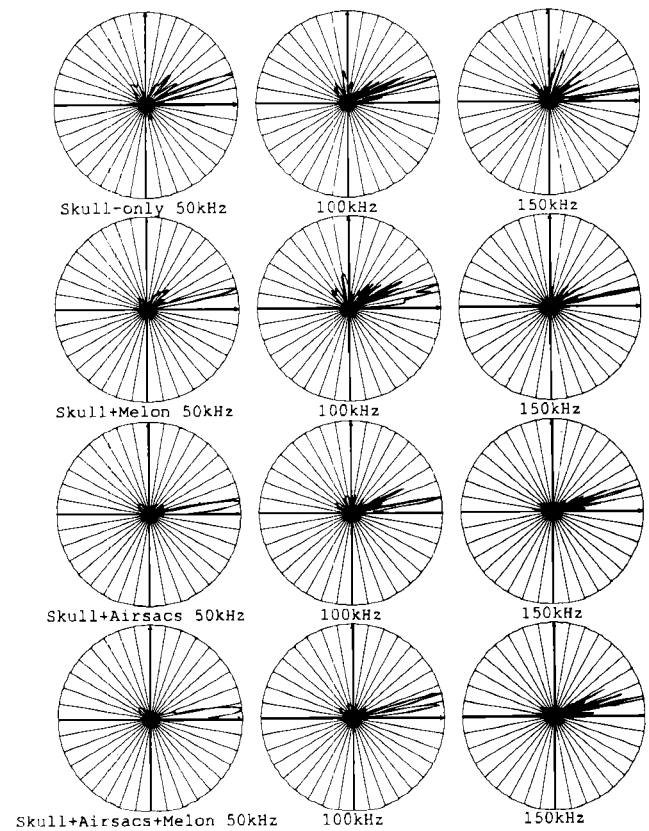

FIG. 8. Collected results. Linear polar plots of acoustic intensity for skull-only, skull and air sacs, skull and melon, and skull and air sacs and melon simulations with MLDB sources of 50, 100, and 150 kHz.

Our choice of sectional plane and source configuration in these simulations was motivated by the following anatomical considerations. Recent studies (Cranford, 1988) using CT imaging techniques show that the melon terminates posteriorly in a complex structure embracing the main nasal passage just ventral to the vestibular sacs. This complex includes two pairs of fatty bursae, one pair associated with each (left and right) side of the airway. Each pair of bursae is also associated with a small cartilagenous rod embedded in the posterior wall of the airway, a stout ligament, and a pair of keratinous lips (the monkey lips). Cranford (1992) has coined the term MLDB (monkey lip/dorsal bursae) complex to refer to this region and proposes that impulse sounds are generated there via a penumatically driven mechanism. The parasagittal section selected for these simulations lies approximately 1 cm to the right of the midsagittal plane of the dolphin head, transecting both the right nasal plug lip and the right bursae of the MLDB complex. The small size of the monkey lips (approximately 3 mm in sagittal section) compared with the shortest wavelength simulated (1 cm) justifies the use of a point source to model this source region over the range of simulated wavelengths. Modeling of the dolphin head in this plane and the use of a point source is relevant to the MLDB source hypothesis (Aroyan, 1990). Other hypotheses may suggest a different choice of anatomical section and source configuration.

The two-dimensional nature of this model neglects variation in the third spatial dimension. However, the selected simulation plane does provide significant qualitative information about the situation in 3-D. Dimensionality is an important issue here, but note that a lens or mirror which focuses in 3-D will also focus in a properly chosen 2-D section. Clearly 2-D simulations cannot provide the level of quantitative precision afforded by modeling in 3-D,[10] but the ease with which various tissue models may be added or removed and source hypotheses tested in these simulations does allow important qualitative exploration to be carried out.

Signals measured in the far field of echolocating dolphins are a product of the interaction of the pulses produced by the dolphin's acoustic source with the surrounding tissues. For this reason we decided not to insert the measured echolocation pulse emitted by the modeled species of dolphin at the source position in the initial simulations. In a summary of several studies, Wood and Evans (1980) listed a peak echolocation pulse frequency range of 20–100 kHz and a maximum hearing sensitivity frequency range of 60–100 kHz for *Delphinus delphis*. In this report, we show results of simulations using a harmonic source signal at a sampling of frequencies: 50, 100, and 150 kHz.[11] One artifact of these monochromatic source frequencies is the multiply spiked appearance of the interference lobes within the overall pattern of the polar intensity plots (e.g., see the 150-kHz plots of Fig. 8).

III. RESULTS OF THE SIMULATIONS

A. Skull-only MLDB source simulations

Figure 1 illustrates the emission pattern resulting from a skull-only simulation with a point source of frequency 100 kHz located in the MLDB complex. Linear polar intensity plots for these simulations at source frequencies of 50, 100, and 150 kHz are included in Fig. 8. The skull-only simulations exhibit a striking degree of forward reflected energy for a point source located in the region of the MLDB complex. Variations in literature values of mammalian bone density and velocity do not strongly affect these patterns.[12] Thus by itself, the skull can function as an acoustical mirror, confirming earlier studies (Evans *et al.*, 1964; Schenkkan, 1973; Dubrovskiy and Zaslavskiy, 1975). However, in view of the fact that air sacs cover much of the skull surface in the vicinity of the nasal passages, it is likely that the focal geometry demonstrated here also serves (perhaps primarily) to shape and support the highly reflective flesh-air boundary.[13]

B. Skull-only moved source simulations

Several experimental techniques have been applied in attempts to pinpoint the location of the click-producing tissues. Evidence from acoustic measurements (Diercks *et al.*, 1971), x-ray studies (Norris *et al.*, 1971; Dormer, 1974, 1979), pressure and muscle activity measurements (Ridgway *et al.*, 1980), pulsed ultrasonic imaging (Mackay, 1980) and Doppler motion detection (Mackay and Liaw, 1981) appears to implicate a region near the nasal plugs as the most likely source location, though a theory identifying the larynx as the site of sound production also has proponents (Purves, 1967; Schenkkan and Purves, 1973; Purves and Pilleri, 1983). In this set of simulations, the dependence of the emitted field on the location of the point source was tested. The source locations tested included the MLDB complex, the nasal plug, and the larynx; see Fig. 2.

We found gross degradation of the forward lobe pattern for sources located far from the MLDB region in our *Delphinus* model.[14] Polar intensity plots for 100-kHz sources located in the nasal plug and larynx regions of the skull-only model are shown in Fig. 3. Major portions of the beam point upward for the nasal plug source location, whereas a larynx source location projects acoustic energy ventrally and not forward. (Similar patterns occur in the skull and air sacs and melon model.) Our results therefore favor the MLDB region, and not the nasal plugs or the larynx, as the site of echolocation click production.

A surprising degree of sensitivity to small source displacements about the MLDB complex was found. Sets of simulations were run at 50, 100, and 150 kHz in both the skull-only and the skull and air sacs and melon models on a grid of source positions over the region of the upper nasal passages. Figure 4 plots polar intensity for a 100-kHz source moved in increments of 0.75 cm around the MLDB complex in the skull-only model, and illustrates that small displacements away from the complex generally cause degradation of the forward pattern.

C. Skull and air sacs simulations

It is generally recognized that air acts as an important acoustical reflector in the delphinid sonar system. Figure 5 shows a simple model of the nasal sacs that was generated from both CT scan and dissection studies.[15] Polar plots of

acoustic intensity for the combined skull and air sacs simulations (with MLDB sources of 50, 100, and 150 kHz) are shown in Fig. 8.[16] The geometry of the sacs (especially those immediately surrounding the source region) strongly influence the emitted pattern. Perhaps reflection from the nasal sacs and from the skull (at higher angles of incidence) is the principle mechanism of beam formation. Our model is neither exact nor complete, however, and these simulations, though suggestive, have not resolved the contribution of the nasal sacs to the formation of the dolphin's sonar beam.[17]

D. Melon-only simulations

Besides the nasal sacs and the skull, the melon may also play a role in echolocation beam formation. Wood (1964) suggested that the melon may both focus and acoustically couple internally generated sound to seawater. Sound speed measurements by Norris and Harvey (1974) on the melon of a Pacific bottlenose dolphin subsequently revealed a low-velocity core and a graded outer shell of high-velocity tissue. In addition, Evans *et al.* (1964) and Romanenko (1974) found that presence of the soft tissue of the dolphin's forehead caused narrower beams to be emitted than were produced by the skull alone. To help distinguish the effect of the velocity lensing from other beam forming mechanisms (e.g., source directivity, tissue interface reflectivity), the sound speed measurements of Norris and Harvey (1974) were used to generate a grid of velocity values over the melon region of our *Delphinus* model. In Fig. 6 we see the effect of this velocity profile (without other tissues) on sources located in the MLDB complex. These simulations demonstrate that a profile of the measured magnitude is capable of mild focusing. By itself, however, this profile could not produce the dolphin's highly directed acoustic beams.

E. Skull and melon simulations

Adding the contoured melon velocity profile to the skull model (with the same frequencies and source location) produces the results shown in Fig. 8. The melon model appears to slightly assist the skull in channeling a larger fraction of the total energy into the main forward lobe. It is clear however that the effects of the skull and air sacs dominate effects due to the melon. From these simulations we conclude only that the measured velocity magnitudes are capable of "fine focusing" the beam reflected from the skull and air sacs.

F. Skull and air sacs and melon simulations

The combined effects of the skull, air sacs, and melon represents the most complete model of dolphin acoustic beam formation attempted in this study. Adding the previously shown air sac configuration to the skull and melon simulations, we obtain the results shown in Figs. 7 and 8. The degree of forward focusing by this model is striking, and beam angles closely approximate those measured by experimental methods.[18]

IV. CONCLUSIONS

Despite the inherent limitations of 2-D modeling and simplification of the elastic properties of tissues, these simulations provide a means for qualitative investigation of acoustic beam formation and source location hypotheses. They contribute to the following picture of sound emission: The skull and air sacs appear to be acting in concert as an acoustical mirror which reflects sound originating from the region of the MLDB complex into highly directed forward beams. A melon velocity profile of the magnitude tested is capable of mild focusing effects, and may serve to "fine focus" the beam formed by the skull and air sacs. We suggest that the dolphin produces echolocation pulses in the vicinity of the MLDB complex (not in the nasal plug or laryngeal regions) and achieves a focused beam pattern through the combined acoustical effects of the skull, air sacs, and melon.

This study far from exhausts the possibilities for investigative computer modeling of dolphin echolocation. Improved tissue velocity and density data would permit more precise simulation of several delphinid species. Simulations with broadband pulses should better localize the source region and may reveal clues of source and surrounding tissue interaction. It also appears that 3-D modeling is feasible, which will permit quantitatively accurate beam simulation and comparison with experimental results. Finally, simulation in 3-D may allow investigation of the mechanisms of directional hearing in delphinids.

ACKNOWLEDGMENTS

Grateful acknowledgment for partial support of this research is made to the UCSC Institute for Nonlinear Science, and to its director, Michael Nauenberg, for his support and early recognition of this research. Special thanks is due John Vidale[19] for many useful discussions of numerical wave propagation. Simulation programs were run on the San Diego Supercomputer Center CRAY Y-MP.

APPENDIX

This Appendix presents pertinent details of the numerical methods utilized in the simulations.[20]

The following discretization of Eq. (1), solved for the numerical value of the acoustic pressure $P_{i,j}^{k+1}$ at the (i,j)th grid position and $(k+1)$th time step, was utilized over the tissue region of the grid.

$$P_{i,j}^{k+1} = (2 - 5\kappa_{i,j}^2)P_{i,j}^{k} - P_{i,j}^{k-1} + \frac{4\kappa_{i,j}^2}{3}(P_{i+1,j}^{k} + P_{i-1,j}^{k} + P_{i,j+1}^{k} + P_{i,j-1}^{k}) - \frac{\kappa_{i,j}^2}{12}(P_{i+2,j}^{k} + P_{i-2,j}^{k} + P_{i,j+2}^{k} + P_{i,j-2}^{k})$$

$$-\frac{h^2\kappa_{i,j}^2}{3\rho_{i,j}}(\rho_{i+1,j}-\rho_{i-1,j})\left((P^j_{i+1,j}-P^k_{i-1,j})-\frac{1}{8}(P^k_{i+2,j}+P^k_{i-2,j})\right)$$
$$-\frac{h^2\kappa_{i,j}^2}{3\rho_{i,j}}(\rho_{i,j+1}-\rho_{i,j-1})\left((P^k_{i,j+1}-P^k_{i,j-1})-\frac{1}{8}(P^k_{i,j+2}+P^k_{i,j-2})\right). \quad \text{(A1)}$$

Here $\kappa_{i,j}\equiv(l/h)c_{i,j}$; $\rho_{i,j}$ and $c_{i,j}$ are the spatially varying density and acoustic velocity; and l and $h=\Delta x=\Delta y$ are the temporal and spatial grid increments, respectively. This scheme is fourth order in the spatial derivatives of pressure, second order in the spatial derivatives of density, and second order in the time derivative of pressure.[21]

Consistency and stability can be shown for the homogeneous scheme [the first two lines of Eq. (A1)] used over the remainder of the grid provided $\kappa_{i,j}=\kappa=(l/h)c\leqslant\sqrt{3/8}$, where c is the sound velocity. Stability of the inhomogeneous scheme additionally requires that density discontinuities not exceed a factor of about 2.5 per grid point; however, the ratio of densities of flesh to air is nearly 10^3. For this technical reason, and because of the high reflectivity of the flesh-air boundary, air sacs were modeled as "pressure release" surfaces; i.e., the pressure was set to zero inside sac contours.

Simulations were conducted on 1100 by 1100 grids of increment size 1.5 mm; grids thus represent square areas of side length 1.65 m. Bone density and velocity were assumed to be 2.0 g/cc and 3450 m/s, respectively. Seawater (and soft tissue, unless otherwise noted) density and velocity were assumed to be 1.0 g/cc and 1500 m/s, respectively.

[1]See, for example, Norris *et al.* (1971), Norris and Evans (1967), Evans (1973), Au (1980), and Au *et al.* (1986).

[2]This problem is closely analogous to the propagation of seismic waves through the complex layers of the Earth's mantle and crust, the simulation of which generally requires solution of the full elastic wave equation.

[3]Density (ρ) and velocity (c) values given in the Appendix imply an acoustic impedance ratio between bone ($r_b=\rho_b c_b$) and soft tissue ($r_{st}=\rho_{st}c_{st}$) of $r_b/r_{st}=4.6$.

[4]Pierce (1981), p. 432. This equation differs from the case for homogeneous fluids only in having an extra term proportional to the gradient of the density field.

[5]The ring of points is located essentially in the far field of the pressure distribution and centered on the apparent source location of the forward beams. Linear polar plots of mean square amplitude are therefore approximately equivalent to plots of energy flow versus angle.

[6]Average values for bone velocity and density were estimated from compilations of (terrestrial) mammalian tissues (e.g., Goss *et al.*, 1980) to be 3450 m/s and 2.0 g/cc. Bone velocity values vary about 15% from the average, and bone density roughly 10% in these compilations.

[7]Velocity and density were set at the background seawater values. Information available from mapping between x-ray absorption values and physical mass density was not utilized in these simulations.

[8]Note that neglecting small density or velocity discontinuities and the elastic characteristics of soft tissue interfaces eliminates the possibility of waveguiding behavior at grazing angles of incidence: cf. Norris (1968).

[9]Midsagittal plane sound speed values measured in the *Tursiops* melon were overlaid onto the *Delphinus* melon region, with the melon boundary assigned to the surrounding (seawater) velocity. Though highly approximate, this procedure is quite useful for investigating the magnitude of the effect of the measured velocity values on acoustic beam formation. From morphologic comparisons, Cranford (1992) found that the melons of *Tursiops* and *Delphinus* are similar in shape though varying in overall size.

[10]We are developing programs for 3-D bioacoustic modeling.

[11]Focusing at discrete frequencies constitutes a necessary but not sufficient condition for broadband focusing. Simulations utilizing broadband source signals are underway.

[12]Variations of $\pm$ 25% in bone density and $\pm$ 15% in bone velocity were tested in Aroyan (1990). The geometry (not the precise reflectivity) of a mirror's surface determines its focal behavior; consider, for example, the mirror of the Hubble space telescope.

[13]The pressure amplitude reflection coefficient for acoustic plane waves normally incident on an air-flesh boundary is approximately 0.9995 (Aroyan, 1990, p. 22). For a flesh-bone interface this coefficient is roughly 0.6 for normal incidence, but increases to unity at a critical angle of about 30 deg.

[14]The MLDB complex lies 2–3 cm dorsal to the nasal plug area in our *Delphinus* model.

[15]CT scans provide accurate information on skull geometry. Because postmortem specimens were scanned, however, only approximate information on the geometry of the sacs was obtained.

[16]Air sacs were modeled as "pressure release" surfaces in the simulations; see the Appendix. Note that potential sac resonances are eliminated by this procedure.

[17]Modeling in 3-D will permit a greatly improved determination of the relative importance of the skull and nasal sacs in beam formation.

[18]Though not measured for *Delphinus*, compare the results of Au *et al.* (1986).

[19]United States Geological Survey, Menlo Park, CA 94025.

[20]The reader is referred to Aroyan (1990) for a more complete discussion of the simulation methods.

[21]Second order spatial derivatives of density were used in order to best simulate boundary behavior at sharp tissue interfaces; see Aroyan (1990), pp. 37–40. In addition, second order paraxial absorbing boundary conditions were added to reduce spurious reflection from grid edges; ref. Clayton and Engquist (1977).

Alford, R. M., Kelly, K. R., and Moore, D. M. (1974). "Accuracy of Finite-Difference Modeling of the Acoustic Wave Equation," Geophysics 39(6), 834–842.

Aroyan, J. L. (1990). "Numerical Simulation of Dolphin Echolocation Beam Formation," M. S. thesis, UC Santa Cruz.

Au, W. W. L. (1980). "Echolocation Signals of the Atlantic Bottlense Dolphin (*Tursiops truncatus*), in Open Waters," in *Animal Sonar Systems*, edited by R. G. Busnel and J. F. Fish (Plenum, New York), pp. 251–282.

Au, W. W. L., Moore, P. W. B., and Pawloski, D. (1986). "Echolocation Transmitting Beam of the Atlantic Bottlenose Dolphin," J. Acoust. Soc. Am. 80, 688–691.

Clayton, R., and Engquist, B. (1977). "Absorbing Boundary Conditions for Acoustic and Elastic Wave Equations," Bull. Seis. Soc. Am. 67, 1529–1540.

Cranford, T. W. (1988). "The Anatomy of Acoustic Structures in the Spinner Dolphin Forehead as shown by X-ray Computed Tomography and Computer Graphics," in *Animal Sonar: Processes and Performance*, edited by P. E. Nachtigall and P. W. B. Moore (Plenum, New York), pp. 67–77.

Cranford, T. W. (1992). "Functional Morphology of the Odontocete Forehead: Implications for Sound Generation," Ph.D. thesis, U.C. Santa Cruz.

Diercks, K. J., Evans, W. E., Trochta, R. T., and Greenlaw, C. F. (1971). "Recording and Analysis of Dolphin Echolocation Signals," J. Acoust. Soc. Am. 49, 1729–1732.

Dormer, K. J. (1974). "The Mechanism of Sound Production and Measurement of Sound Processes in Delphinid Cetaceans," Ph.D. thesis, UC Los Angeles.

Dormer, K. J. (1979). "Mechanism of Sound Production and Air Recycling in Delphinids: Cineradiographic Evidence," J. Acoust. Soc. Am. 65, 229–239.

Dubrovskiy, N. A., and Zaslavskiy, G. L. (1975). "Dolphin Echolocation:

Skull Bone, Dolphin Sounding Pulse," Akust. Zh. **21**(3) (Joint Publications Research Service, Arlington, VA, JPRS-65777).

Evans, W. E., Sutherland, W. W., and Beil, R. G. (**1964**). "The Directional Characteristics of Delphinid Sounds," in *Marine Bioacoustics*, edited by W. N. Tavolga (Pergamon, New York), pp. 353–372.

Evans, W. E. (**1973**). "Echolocation by Marine Delphinids and One Species of Fresh-Water Dolphin," J. Acoust. Soc. Am. **54**, 191–199.

Goss, S. A., Johnston, R. L., and Dunn, F. (**1980**). "Compilation of Empirical Ultrasonic Properties of Mammalian Tissues. II," J. Acoust. Soc. Am. **68**, 93–108.

Litchfield, C., Karol, R., Mullen, M. E., Dilger, J. P., and Luthi, B. (**1979**). "Physical Factors Influencing Refraction of the Echolocative Sound Beam in Delphinid Cetaceans," Mar. Biol. **52**, 285–290.

Mackay, R. S. (**1980**). "Dolphin Air Sac Motion Measurements During Vocalization by Two Noninvasive Ultrasonic Methods," in *Animal Sonar Systems*, edited by R. G. Busnel and J. F. Fish (Plenum, New York), pp. 933–937.

Mackay, R. S., and Liaw, H. M. (**1981**). "Dolphin Vocalization Mechanisms," Science **212**, 676–677.

Norris, K. S., and Evans, W. E. (**1967**). "Directionality of Echolocation Clicks in the Rough Tooth Porpoise *Steno bredanensis* (Lesson)," in *Proceedings of 2nd Conference on Marine Bio-acoustics*, edited by W. N. Tavolga (Am. Mus. of Nat. Hist., New York).

Norris, K. S. (**1968**). "The Evolution of Acoustic Mechanisms in Odontocete Cetaceans," in *Evolution and Environment*, edited by E. Drake (Yale U. P., New Haven, CT), pp. 297–324.

Norris, K. S., Dormer, K. J., Pegg, J., and Liese, G. T. (**1971**). "The Mechanism of Sound Production and Air Recycling in Porpoises: A Preliminary Report" (Dept. Zool., Oceanic Inst., Waimanalo, HI; Oceanic Inst. UCLA, Queen's Med. Cen., Honolulu, HI), Contribution No. 90.

Norris, K. S., and Harvey, G. W. (**1974**). "Sound Transmission in the Porpoise Head," J. Acoust. Soc. Am. **56**, 659–664.

Pierce, A. D. (**1981**). *Acoustics: An Introduction to its Physical Principles and Applications* (McGraw-Hill, New York).

Purves, P. E. (**1967**). "Anatomical and Experimental Observations on the Cetacean Sonar System," in *Animal Sonar Systems: Biology and Bionics*, edited by R. G. Busnel (Laboratoire de Physiologie Acoustique, Jouy-en-josas-78, France), Vol. 1, pp. 197–270.

Purves, P. E., and Pilleri, G. (**1983**). *Echolocation in Whales and Dolphins* (Academic, New York).

Ridgway, S. H., Carder, D. A., Green, R. F., Gaunt, A. S., Gaunt, S. L. L., and Evans, W. E. (**1980**). "Electromyographic and Pressure Events in the Nasolaryngeal System of Dolphins During Sound Production," in *Animal Sonar Systems*, edited by R. G. Busnel and J. F. Fish (Plenum, New York), pp. 239–249.

Romanenko, Y. V. (**1974**). *Physical Fundamentals of Bioacoustics* (Fizicheskiye Osnovy Bioakustik) (Joint Publications Research Service, Arlington, VA, JPRS-63923).

Schenkkan, E. J. (**1973**). "On the Comparative Anatomy and Function of the Nasal Tract in Odontocetes (Mammalia, Cetacea)," Bijdragen tot de Dierkunde **43**(2), 127–159.

Schenkkan, E. J., and Purves, P. E. (**1973**). "The Comparative Anatomy of the Nasal Tract and Function of the Spermaceti Organ in the Physeteridae (Mammalia: Odontoceti)," Bijdragen tot de Dierkunde **43**(1), 93–112.

Varanasi, U., Markey, D., and Malins, D. C. (**1982**). "Role of Isovaleroyl Lipids in Channeling of Sound in the Porpoise Melon," Chem. Phys. Lipids **31**, 237–244.

Wood, F. G. (**1964**). In *Marine Bio-acoustics*, edited by W. N. Tavolga (Pergamon, New York), p. 309.

Wood, F. G., and Evans, W. E. (**1980**). "Adaptiveness and Ecology of Echolocation in Toothed Whales," in *Animal Sonar Systems*, edited by R. G. Busnel and J. F. Fish (Plenum, New York), pp. 381–426.